Int. J. Electrochem. Sci., 14 **(2019)** 11641 – 11650, doi: 10.20964/2019.12.06

International Journal of ELECTROCHEMICAL SCIENCE
www.electrochemsci.org

Short Communication

Epoxy/Nano-SiO_2 Anticorrosion Coatings Synthesized by Different Molar Ratio of Tetraethyl orthosilicate (TEOS) and Tetramethyl orthosilicate (TMOS)

Shaoxiang Li[1,2,3], *Jiaping Wang*[1,2,3], *Wenjuan Qu*[1,2,3,*], *Jiaji Cheng*[1,2,3], *Yunna Lei*[1,2,3], *Meng Liu*[1,2,3], *Dong Wang*[1,2,3]

[1] College of Environment and Safety Engineering, Qingdao University of Science and Technology, Qingdao, 266042, P. R. China
[2] Shandong Engineering Research Center for Marine Environment Corrosion and Safety Protection, Qingdao University of Science and Technology, Qingdao, 266042, P. R. China
[3] Shandong Engineering Technology Research Center for Advanced Coating, Qingdao University of Science and Technology, Qingdao, 266042, P. R. China
[*]E-mail qwj_710@163.com

Received: 24 June 2019 / *Accepted:* 12 August 2019 / *Published:* 29 October 2019

Epoxy/nano-SiO_2 composite coatings were carried out by using epoxy with different TEOS/TMOS molar ratio. Nano-silica particles, which were synthesized by different molar ratio of tetraethyl orthosilicate (TEOS) and tetramethyl orthosilicate (TMOS), manifested different characteristics in particle size and modifier graft coverage. The structure was analyzed by FT-IR, XRD and SEM. The particle size of the silica was correspondingly reduced and the surface coverage of the APTES decreased with the TMOS content reduced. Thus, the particle size and surface coverage of the APTES play an important role in corrosion resistant of epoxy/nano-SiO_2 composite coatings. The results showed that the composite coating had the best anticorrosion effect when the molar ratio of TEOS / TMOS was 1: 1.

Keywords: Epoxy coatings; Nano-silica; Nanoparticles; Corrosion

1. INTRODUCTION

It is well known that coating is the most effective and direct method of preventing metals from corrosion [1-6]. Epoxy anticorrosion coatings were widely used due to their excellent chemical, corrosion resistance, room temperature curing and good adhesion [7-9]. Nevertheless, epoxy anticorrosion coatings have poor weather resistance, brittleness, adhesion loss and unstable corrosion resistance at high temperature, which limits its application for high performance coatings [10]. In recent

years, relatively many studies have focused on the nano-modification to meet the development needs of epoxy anticorrosion coatings [11-13]. Nanoparticles can promote the crosslinking reaction of epoxy resin and enhance the compactness of coating.

Nano-silica is possessed of the singular properties of small size effect, surface interface effect, quantum size effect, macroscopic quantum tunneling effect and electrical characteristics, which is one of the most important nanoparticles [14-17]. Moreover, it is non-toxic, non-pollution and three-dimensional network structure. Consequently, epoxy/nano-SiO_2 composite coating exhibit a good adhesion force, a strong resistance against permeation and excellent anticorrosion behavior [18-20]. Malaki explored the effect of nano-silica on the mechanical properties of acrylic polyurethane coatings, finding that nano-silica additives significantly improved the adhesive strength, and highly increased the micro-hardness as well as the erosion resistance [21]. Chruściel investigated modifications of epoxy resins with nano-silica and concluded that nano-silica could improve mechanical properties, thermal and flame resistance as well as provide corrosion and antimicrobial protection [18]. Though epoxy/nano-silica anticorrosion coatings were used in anticorrosion, there is no direct report aimed at the coatings which were prepared by different proportion of TEOS/TMOS.

In this paper, on the basis of St¨ober method [22-26], nano-SiO_2 particles were prepared with different molar ratio of TEOS/TMOS. Then, nano-silica was modified by silane coupling agent 3-aminopropyl triethoxysilane (APTES). The average particle diameter and the structure were analyzed by laser particle size analyzer, FT-IR and XRD. Then the anticorrosion coatings of epoxy/nano-SiO_2 with different proportions of TEOS/TMOS were prepared and the corrosion resistance was analyzed by electrochemical impedance spectra (EIS).

2. EXPERIMENTAL

2.1. Materials

Tetraethyl orthosilicate (TEOS), tetramethyl orthosilicate (TMOS), 3-aminopropyltriethoxysilane (KH550), ammonia(25%), absolute ethanol, titanium pigment and barium sulfate powder were purchased from Sinopharm Chemical Reagent Co.,Ltd. Waterborne epoxy emulsion (STW703A), aqueous rheological additives (WT202), waterborne epoxy curing agent (STW703B) and propylene glycol methyl ether acetate (PMA) used in this research were supplied by Shanghai Hua Yi Group Company.

2.2. Preparation of nano-SiO_2

Ethanol, deionized water and ammonium hydroxide were mixed in a three-necked flask. TEOS, TMOS (the molar ratio of TMOS:TEOS were 3:1, 2:1, 1:1, 1:2 labeled as 1#, 2#, 3#, 4#) and ethanol were added into the mixture under mechanical stirring for twelve hours. APTES solution (10wt.% in absolute ethanol) was added for 30 minutes and then stirred for 6h at 50℃. The resulting silanized SiO_2 (r-SiO_2 1#, 2#, 3#, 4#) were filtered, dried in oven.

2.3. Preparation of epoxy/nano SiO_2 anticorrosion composite coatings

A certain amount of waterborne epoxy (703A), titanium pigment, barium sulfate aqueous, rheological additives (WT202), propylene glycol methyl ether acetate (PMA) and as-prepared r-SiO_2 (2 wt.% based on composites) were stirred at the speed of 1000r/min, then component A was obtained. Then appropriate amount of 703B resin (epoxy curing agent) and deionized water were mixed to compose a curing agent component B. Finally, the components A and B were mixed, thus an aqueous coating of the epoxy resin was obtained. The anticorrosion coatings of epoxy/nano-SiO_2 (1#, 2#, 3#, 4#) were prepared by using r-SiO_2 (2wt.% based on composites) as filler.

2.4. Characterizations

Operating in the reflection mode with Cu-Kα radiation (35 kV, 30 mA), XRD measurements were performed on the Bruker D8 Advance diffractometer with the step of 0.075° (2θ) and 4 s per step. Diluted with ethanol and dispersed by ultrasonic for 10 min, the particle diameter was measured by a laser particle size analyzer (BIC-9010, Brookhaven Instrument Co.,Holtsville, New York). Using the KBr pellet method, fourier transform infrared (FTIR) spectra of SiO_2 and r-SiO_2 samples were obtained between 4000 and 400 cm^{-1} with an FTIR spectrometer (TENSOR27, BRUKER, Germany). A minimum of 32 scans was signal-averaged with a resolution of 2 cm^{-1}. SEM was performed on a SEM instrument (S-4800, Hitachi Corp., Tokyo, Japan) to characterize the morphology of as-prepared nano-silica. The accelerated voltage was 15 kV. The specific surface area was determined by Quantachrome Instruments U.S. Measurements of organic carbon were carried out with a TOC-A (Total Organic Carbon Analyzer). The carbon concentration measured was then converted into quantity of APTES present on the silica surface by calculating the percentage of carbon in APTES. All electrochemical tests were performed using AMETEK Parstat 4000 workstation. The electrochemical tests were conducted in 3.5 wt.% NaCl aqueous solution with a classical three-electrode system at room temperature. A three-electrochemical cell was constructed with the Q235B carbon steel electrode with coating as working electrode, a saturated calomel electrode (SCE) as reference electrode and a platinum plate as counter electrode. To attain the stabilized open circuit potential (OCP), the working electrodes were immersed in 3.5 wt.% NaCl solution for 20 min before to start the measurements. The OCP of different coatings processed with different immersion time were measured. Then the EIS was measured with a sinusoidal potential perturbation of 10 mV (peak to peak) in the frequency range from 100 KHz to 10 mHz. The EIS data were fitted by Zview software with an equivalent circuit.

3. RESULTS AND DISCUSSION

Fig. 1 (a) depicted the XRD pattern of sample. The obviously broadened diffraction peak at ca.20° was a typical XRD character of amorphous materials. The FT-IR spectra of SiO_2 and r-SiO_2 were shown in Fig. 1 (b). The strong absorption band at 797 cm^{-1}, 1119 cm^{-1} corresponded to the Si-O-Si symmetric stretching vibration and asymmetric stretching absorption peaks respectively. The absorption

peak at 458 cm^{-1} corresponded to the bending vibration of Si-O-Si. The vicinity of 950 cm^{-1} was the result of the bending vibration absorption peak of Si-OH. It showed that nano-SiO_2 has been prepared successfully by sol-gel method. After modified with APTES, as seen in the spectrum of r-SiO_2, the absorption peak for –OH groups became weak and new peak at 3100 cm^{-1} corresponding to the stretching vibration of N-H was observed, which suggested the reducing of Si-OH structural unit. Meanwhile, peaks of methylene emerge at 2950 cm^{-1} and 1148 cm^{-1} demonstrated that the nano-SiO_2 has been successfully modified by APTES and interacted with it.

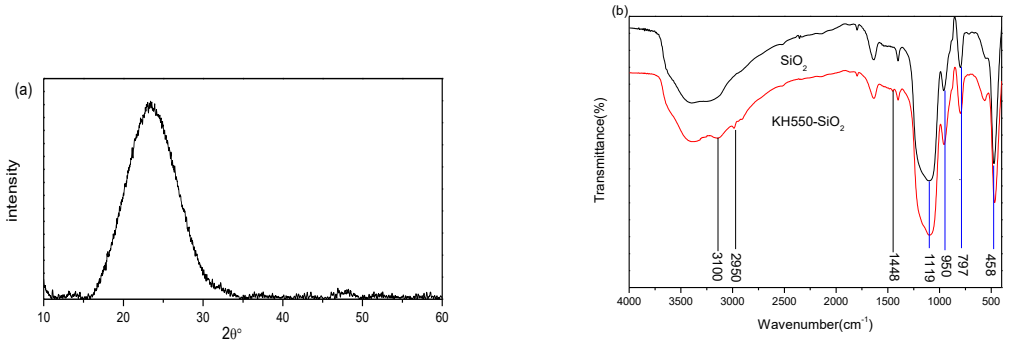

Figure 1. (a) XRD pattern of as-prepared SiO_2, (b) the FT-IR spectra of SiO_2 and r-SiO_2 modified by APTES

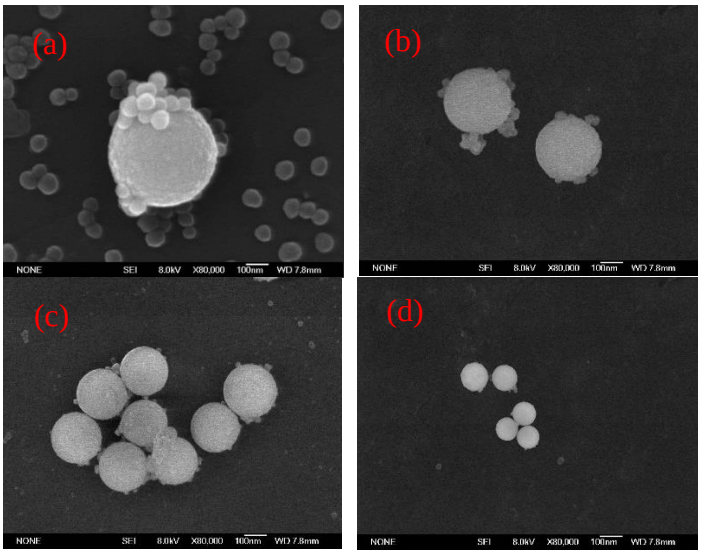

Figure 2. SEM images of r-SiO_2 samples prepared by different proportion of TEOS/TMOS 1# (a), 2# (b), 3# (c), and 4# (d)

Fig. 2 showed SEM images of r-SiO_2 samples. It could be seen that the particle size of the silica was correspondingly reduced from 450 nm to about 100 nm, as the TMOS content in the silica precursor was reduced. The particle size distribution, which was showed in Fig. 3, may reflect the change in particle size more clearly. Moreover, the almost invisible protuberances which were formed by the

polymerization of the modifier on the surface of the silica microspheres became less, as the TMOS content decreased. This may be due to the gradually reduce of surface coverage of APTES.

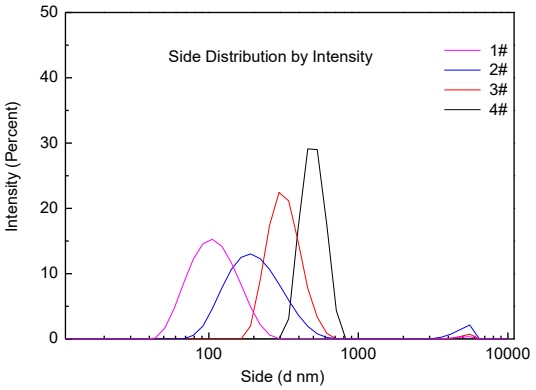

Figure 3. The particle size of silica particles prepared by different proportion of TEOS/TMOS

The carbon concentration (TOC) was measured by calculating the percentage of carbon in APTES (Eq. (1)) [27].

$$\chi = \frac{\alpha}{\beta \times \delta \times \mu \times \nu} \qquad \text{Eq. (1)}$$

Where χ is the quantity of APTES on silica (mol/m^2), where α is the mass of carbon in the sample (g), where β is the molar mass of APTES (g/mol), where δ is the percentage of carbon in APTES (%), where μ is the mass of the sample (g), and where ν is the specific surface area of the silica (m^2/g).

The result of the specific surface area test was presented in Table 1. As the TMOS content decreased, the specific surface area of the resulting silica microspheres gradually increased from 87.3 m^2/g to 221.4 m^2/g. Fig. 4 showed the calculation results of APTES surface coverage of different SiO_2 microspheres. Obviously, the APTES coverage of the synthetic SiO_2 microspheres decreased from 3.5×10^{-6} mol/m^2 to 2.1×10^{-6} mol/m^2, when the TMOS content decreased. This was consistent with the SEM and particle size results.

Table 1. Bet surface area of SiO_2 samples prepared by different proportion of TEOS/TMOS

Nu.	**1#**	**2#**	**3#**	**4#**
Bet surface area (m^2/g)	87.3	123.8	186.9	221.4

A model was presented to explain the result as following. Q_i^j was defined to give a more visual interpretation, where Q denoted a tetrafunctional silicon site, the subscript i represented type of the monomer (1 corresponded to TMOS, 2 corresponded to TEOS), the superscript j was the number of silanol bonds on the Si atom. The hydrolysis of TMOS and TEOS contained four kinds of hydrolyzed product, as well as, the order of hydrolysis velocity was $Q_i^3<Q_i^2<Q_i^1<Q_i^0$, $Q_2^j<Q_1^j$. As the concentration of TMOS and TEOS decreased, less Q_i^4 which was the core of the particles was formed. Thus, a few Q_i^3 and Q_i^2 began to participate in the reaction and generated active oligomers.

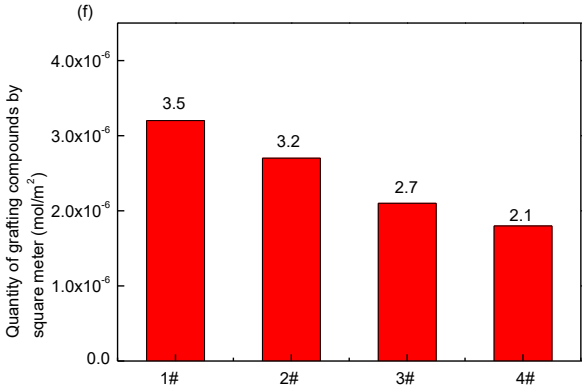

Figure 4. Concentration of APTES

The force including chemical bond and van der walls force may enable two oligomers engulf into each other to keep spherical shape when two oligomers reacted with each other. Evidently, the number of Q_1^4, Q_1^3, Q_1^2 is greater than the corresponding Q_2^4, Q_2^3, Q_2^2, because of the difference in hydrolysis capacity. Thus, the more the molar ratio of TMOS, the larger the particle size of the produced silica was. On the other hand, the oligomer and SiO_2 microspheres produced by more TMOS content contained more silanol bonds, then it was relatively easy to graft with the APTES.

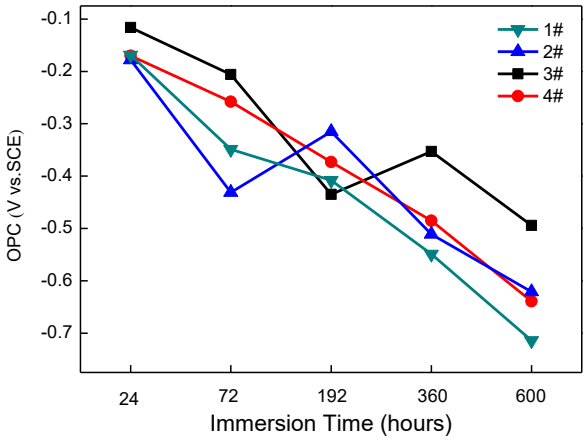

Figure 5. The OCP values of coatings at various immersion time

Open circuit potential (OCP) is a physical quantity that characterizes the corrosion probability of material [28,29]. The OCP plots shown in Fig. 5 displayed a variations in Ecorr with time for the different coatings processed with different immersion time in 3.5 wt.% NaCl solution. The OCP values of all specimens were negative and less than −0.2 V at the initial immersion, which was possibly related with the type of epoxy resin. For the waterborne epoxy resin, water was an excellent catalyst for the amine/epoxy reaction. And the waterborne epoxy coating was more likely to interact with water when it was exposed to the corrosive medium, thus leading to negative OCP value. A higher OCP value usually indicated a lower corrosion tendency [30]. It could be found that all OCP values decreased gradually

with the increasing immersion time. It was mainly because that the composite coatings were penetrated by corrosive medium. Obviously, the OCP values of 3# coating was much higher than others, indicating that the addition of r-SiO_2 (TEOS: TMOS of 1:1) in epoxy coating could decrease the tendency of corrosion.

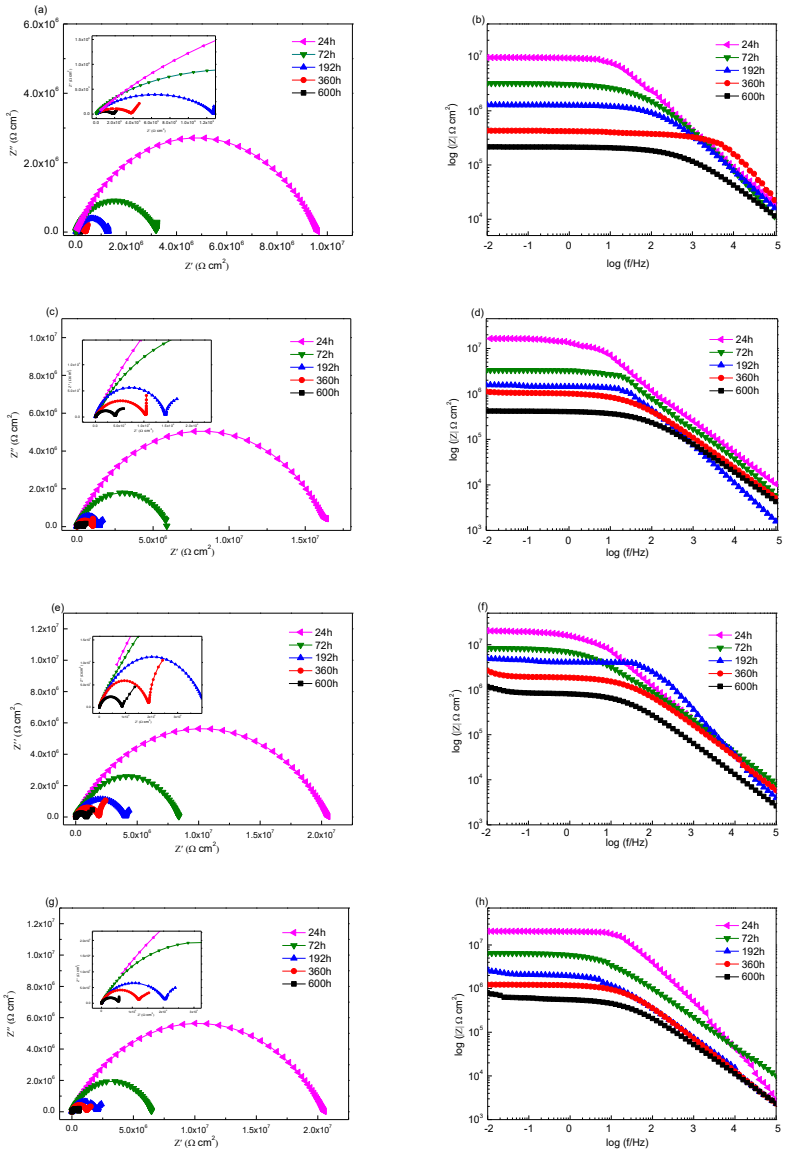

Figure 6. Nyquist and Bode diagrams of EIS measurements performed on different coatings 1# (a, b), 2# (c, d), 3# (e, f), and 4# (g, h)

Electrochemical impedance spectra (EIS) was used to evaluate the electrochemical properties and anticorrosion ability of composite coatings. Fig. 6 showed the Nyquist and Bode plots of different coating systems. For 1# coating, there were two capacitive loops after immersion 24 h (Fig. 6. a). Relatively, two capacitive loops were observed for all coatings after immersion 72 h (Fig. 6. c, e and g). It indicated a longer time, which electrolyte had penetrated the film and reached the contact interface between epoxy coating and steel for 2#, 3# and 4# coatings. Meanwhile, the capacitive loop of all specimens presented a contractive trend as the increase of immersion time, indicating a decline in

corrosion resistance [31]. Moreover, 3# coating possessed the largest semicircle diameter in the Nyquist plot, which suggested the best performance of corrosion resistance.

For the Bode plots, the impedance modulus at low frequency was used to judge the ability of coatings to prevent corrosion [32]. Generally, on account of the permeation of corrosion medium, impedance value decreased with the increase of immersion time. As showed in Bode plots, the initial (24h) impedance value of 1#, 2#, 3#, and 4# specimens were 9.61×10^6 Ω cm^2, 1.64×10^7 Ω cm^2, 2.14×10^7 Ω cm^2 and 2.05×10^7 Ω cm^2 respectively, hinting an obviously protective effect to bare substrate. The final (600h) impedance value of 1#, 2#, 3# and 4# specimens were reduced by 1–3 orders of magnitude to 2.15×10^5 Ω cm^2, 4.20×10^5 Ω cm^2, 1.18×10^6 Ω cm^2 and 7.74×10^5 Ω cm^2 respectively (Fig. 6. b, d, f and h). In addition, the impedance value of 3# coating at different immersion time was evidently higher than other coatings. These observations indicated that the corrosion resistance of 3# coating was the best.

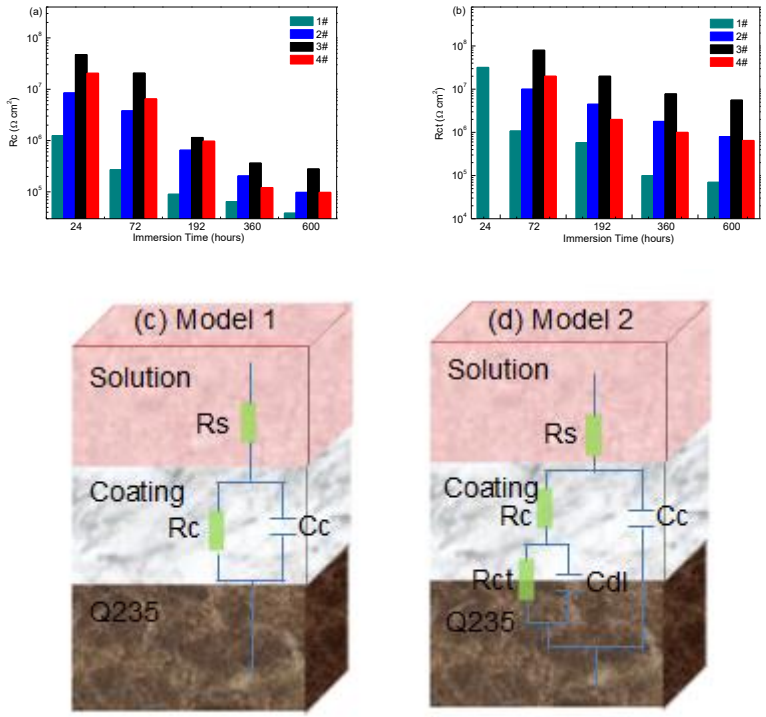

Figure 7. The Rc (a) and Rct (b) of all coating systems at various immersion time and electrical equivalent circuit models (c, d)

Electrical equivalent circuits (EEC) showed in Fig. 7 were employed to interpret the impedance responses, obtaining the best numerical fits for all the EIS results [33-35]. The software named ZSimpWin was used to obtain an equivalent circuit model [36]. EEC contained five parts of Rs, Rc, Rct, Cc and Cdl, corresponding to the solution resistance between working electrode and reference electrode, the pore resistance of coating, the charge-transfer resistance between steel surface and solution interface, the coating capacitance, the double-layer capacitance between steel surface and electrolyte interface, respectively [37,38]. In theory, with the adsorption of corrosion medium, the Rc and Rct value dropped gradually. Rc could evaluate the shielding properties of a coating, while Rct was usually used to characterize the charge transfer resistance of the Q235B steel surface, which was inversely proportional to the corrosion rate. After immersing the 1# coating for 24h and 2#, 3#, 4# coatings for 72h, as

mentioned above, electrolyte had not penetrated the film, these situations were consisted with model 1 (Fig. 7.c). Other situations belonged to model 2 (Fig. 7.d). The value of RC decreased indicating that the shielding properties of all coatings were gradually declined, with the extending of immerse time (Fig. 7. a, b). As well as, the Rct value and Rc value of different coating systems had similar trends. In contrast, both the Rc and Rct value of 3# coating was always higher than that of other coatings. Therefore, the shielding performance of 3# coating was dramatically better while corrosion rate of substrate was lower than others.

From the foregoing, the condensation polymerization reaction rate and the size of silica decreased with the decrease of TMOS content in the silicon source. This was beneficial to improve the corrosion resistance of the coating. However, the adhesive force and compactness of coating became worse when the content TMOS was too little. Additionally, when the content of TMOS in the silicon source was high, the silica possessed of good silane grafting density. The nano-silica modified by APTES can easily interact with epoxy groups, and then promote the crosslinking reaction of epoxy resin and enhance the compactness of coating. Moreover, it can increase the corrosion resistance of epoxy coatings via the formation of Fe-O-Si covalent bond at the interface of metal/coating [39]. But the content of TMOS in the silicon source was too high, the particle size of the produced silica was large, causing severe agglomeration when used in coatings Therefore, the corrosion resistance of the coating was the result of a combination of particle size and surface coverage of the APTES. The results showed that epoxy/nano-SiO_2 composite coatings had the best anticorrosive property when the TEOS and TMOS ratio in the silicon source was 1:1.

4. CONCLUSIONS

Epoxy/nano-SiO_2 composite coatings with different proportion of TEOS/TMOS were successfully fabricated. The results of SEM, DLS, BET and TOC suggested that the larger the particle size of the prepared silica was, the smaller of the specific surface area would become, and the surface coverage of the APTES increased with the molar ratio of TMOS increased. But the corrosion resistance of the coating was the result of both the combination of particle size and surface coverage of the APTES. The epoxy/nano- SiO_2 composite coatings had the best anticorrosive property when the proportion of TEOS/TMOS was 1:1.

ACKNOWLEDGEMENTS
This work was financially supported by Natural Science Foundation of Shandong Province, China (No. ZR2016EMB20), National Natural Science Foundation of China (Grant No.51806113) and Postdoctoral Applied Research program Fund of Qingdao (No. 2016204).

References

1. N. Jadhav, C.A. Vetter and V.J. Gelling, *Electrochim. Acta*, 102 (2013) 28.
2. X. Yuan, Z.F. Yue, X. Chen, S.F. Wen, L. Li and T. Feng, *Corros. Sci*., 104 (2016) 84.
3. A. Shadravan, Z. Sadeghian, A. Nemati and S.P. Mohammadi, *Surf. Coat. Technol*., 275 (2015)224.
4. S. Niroumandrad, M. Rostami and B. Ramezanzadeh, *Prog. Org. Coat*., 101 (2016) 486.
5. S. Mohammadi, H. Shariatpanahi, F.A. Taromi and J. Neshati, *Mater. Res. Bull*., 80 (2016) 7.

6. X. D. Lv, X. T. Li, N. Li, H.C. Zhang, Y.Z. Zheng, J.J. Wu, and X. Tao, *Surf. Coat. Technol*., 358 (2019) 443.
7. F. Galliano and D. Landolt, *Prog. Org. Coat*., 44 (2002) 217.
8. M. Conradi, A. Kocijan, M. Zorko and I. Verpoest, *Prog. Org. Coat*., 80 (2015) 20.
9. N. Moazeni, Z. Mohamad, N.L.I. Faisal, M.A. Tehrani and N. Dehbari, *J. Appl. Polym. Sci.*, 130 (2013) 955.
10. F.L. Jin, X. Li and S.J. Park, *J. Ind. Eng. Chem. (Amsterdam, Neth.),* 29 (2015) 1.
11. H. Ma, X. Zhang, F. Ju and S.B.J.S.R. Tsai, *Sci. Rep*., 8(1) (2018) 3045.
12. Y. Han, A. Taylor and K.M. Knowles, *Surf. Coat. Technol*., 203 (2009) 2871.
13. Y. Hao, X.Y. Zhou, J.J. Shao and Y.K. Zhu, *Surf. Coat. Technol*., 362 (2019) 213.
14. X. Ma, L. Xu, W. Wang, Z. Lin and X. Li, *Corros. Sci.,* 120 (2017) 139.
15. H. Shi, L. Wu, J. Wang, F. Liu and E.H. Han, *Corros. Sci*., 127 (2017) 230.
16. J.B. Xu, Y.Q. Cao, L. Fang and J.M. Hu, *Corros. Sci*., 140 (2018) 349.
17. S. Xu, L. Chen, M. Gong, X. Hu, X. Zhang and Z.J.C.P.B.E. Zhou, *Composites Part B,* 111 (2017) 143.
18. J.J. Chruściel and E. Leśniak, *Prog. Polym. Sci*., 41(2015) 67.
19. M. Conradi, A. Kocijan, D. Kek-Merl, M. Zorko and I.J.A.S.S. Verpoest, *Appl. Surf. Sci.*, 292 (2014) 432.
20. R.N. Peres, E.S.F. Cardoso, M.F. Montemor, H.G. de Melo, A.V. Benedetti and P.H. Suegama, *Surf. Coat. Technol*., 303 (2016) 372.
21. M. Malaki, Y. Hashemzadeh and M. Karevan, *Prog. Org. Coat*., 101 (2016) 477.
22. W. Yu, J. Fu, L. Chen, P. Zong, J. Yin, D. Shang, L. Qi and C. Hua, *Compos. Sci. Technol*., 125 (2016) 90.
23. W. St¨ober, A. Fink, and E. Bohn, *J. Colloid Interface Sci*., 26.1(1968) 62.
24. K.J. Klabunde, J. Stark, O. Koper, C. Mohs, D.G. Park, S. Decker, Y. Jiang, I. Lagadic and D.J.T.J.o.P.C. Zhang, *J. Phys. Chem*., 100 (1996) 12142.
25. G. H. Bogush, M. A. Tracy, and C. F. Zukoski, *J. Non-Cryst. Solids*, 104 (1988) 95.
26. C. J. Brinker and G. W. Scherer, *Adv. Mater. (Weinheim, Ger.)*, 3 (10) (1991) 522.
27. F. Cuoq, A. Masion, J. Labille, J. Rose, F. Ziarelli, B. Prelot and J.-Y.J.A.S.S. Bottero, *Appl. Surf. Sci.,* 266 (2013) 155.
28. Y. Ye, Z. Liu, W. Liu, D. Zhang, H. Zhao, L. Wang and X. Li, *Chem. Eng. J. (Amsterdam, Neth.),* 348 (2018) 940.
29. S. Akhtar, A. Matin, A.M. Kumar, A. Ibrahim and T. Laoui, *Appl. Surf. Sci*., 440 (2018) 1286.
30. Y. Ye, H. Zhao, C. Wang, D. Zhang, H. Chen and W. Liu, *Appl. Surf. Sci.,* 457 (2018) 752.
31. Y. Dun, X. Zhao, Y. Tang, S. Dino and Y.J.A.S.S. Zuo, *Appl. Surf. Sci*., 437 (2018) 152.
32. C. Liu, R.I. Revilla, Z. Liu, D. Zhang, X. Li and H.J.C.S. Terryn, *Corros. Sci*., 129 (2017) 82.
33. S. Ammar, K. Ramesh, B. Vengadaesvaran, S. Ramesh and A.K. Arof*, Prog. Org. Coat*., 92 (2016) 54.
34. X. Yuan, Z.F. Yue, X. Chen, S.F. Wen, L. Li and T. Feng, *Prog. Org. Coat.,* 86 (2015) 41.
35. A. Mostafaei and F. Nasirpouri, *Prog. Org. coat*., 77 (2014) 146.
36. S. Surviliene, A. Lisowska-Oleksiak and A. Češuniene, *Corros. Sci*., 50 (2008) 338.
37. S. Yuan, B. Liang, Y. Zhao and S.O. Pehkonen, *Corros. Sci*., 74 (2013) 353.
38. W. Kwon, J. M. Kim and S. W. Rhee, *Electrochim. Acta*, 68 (2012) 110.
39. K.C. Chang, H.F. Lin, C.Y. Lin, T.H. Kuo, H.H. Huang, S.C. Hsu, J.M. Yeh, J.C. Yang and Y.H. Yu, *J. Nanosci. Nanotechnol*., 8 (2007) 1.